Macromolecules

pubs.acs.org/Macromolecules
Article

Micelle Forming Linear−Dendritic Block Copolymers: A Theoretical Comparison between Random Hyperbranched and Precise Dendrimer Polymer Architectures

Marios Giannakou,* Oleg Borisov,* and Friederike Schmid*

Cite This: *Macromolecules* 2025, 58, 5872−5882
Read Online

ABSTRACT: Hyperbranched block copolymers offer a simpler and more efficient synthesis route compared to more traditional dendritic systems while still providing exceptional control over surface functionality and self-assembly. This makes them ideal candidates for engineering nanoparticles with tailored properties for applications such as drug delivery and sensing. Here we use self-consistent field calculations to compare the micelle structures formed by copolymers with polydisperse hyperbranched (LHBC), monodisperse dendritic (LDBC), and linear solvophilic blocks. Representative LHBC structures were generated by molecular dynamics simulations mimicking the slow-monomer addition protocol. We find that LHBC micelles are more stable, have a lower critical micelle concentration, and are better at accommodating larger drug payloads than LDBC micelles, and these properties further improve with increasing polydispersity. LHBC micelles also offer more terminal ends for functionalization than LDBC micelles for LDBCs with up to four branching generations, with the number of terminal ends being surprisingly independent of the LHBC polydispersity. Our findings highlight the superiority of LHBC micelles in flexibility and performance over LDBC micelles.

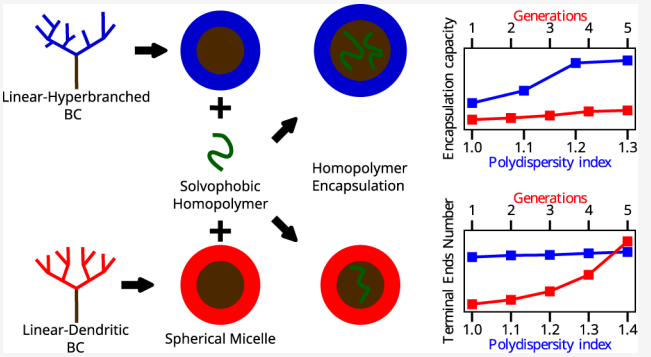

1. INTRODUCTION

Block copolymers have seen a long and sustained interest, both in experiments and theory, mainly due to their ability to self-assemble into a variety of nanoassemblies. This ability stems from the fact that the constituting blocks of the polymers are made from different types of often incompatible monomers that would like to demix, however due to the connectivity of the blocks they instead microphase separate.[1] In the melt regime, for example, even the simplest type of block copolymer, the linear diblock polymer, can self-assemble into a variety of periodic structures like lamellar, hexagonal, spherical, gyroid, and more[1−5] with a periodicity determined largely by the macromolecular weight of the molecules themselves and thereby in the nanoscale range,[1,6,7] Such a capability is highly desired in a range of applications, such as surface pattering,[8] thin films,[9,10] filtration,[11] and many more.[12,13] On the other hand, if a solvent is present that is selective toward one of the types of blocks, but poor toward the others, then the polymers may self-assemble into a variety of states depending on the concentration of the polymers, the molecular weight of the polymer, and other parameters.[14] Some common examples include spherical micelles, elongated micelles, worm-like micelles, or vesicles.[4,15−17] Such structures have been intensely investigated and have a wide range of applications, e.g., in solubilization,[18] stabilization,[19] as nanoreactors[20] for drug encapsulation and delivery,[21,22] and many others.[23] In the present article, we focus on polymeric micelles, which hold promise as nanocarriers for encapsulating and transporting drugs. Micelles do this by incorporating the often hydrophobic drug[22] into their cores, thus solubilizing and protecting it from the highly complex environment *in vivo*.[13] In addition, as drugs need to circulate in the body for some time to reach their target sites, it is vital that the drug release from the nanocarrier happens over hours and not immediately[13] after administration. After entering the bloodstream, the nanoparticles find themselves in a highly dilute environment, much below the critical micelle concentration (CMC), whereupon they disassemble quickly and thus release their drug payload. Polymeric micelles, on the other hand, have a relatively low critical micelle concentration, which enhances their stability and slows down their disassembly to a large extent.[24] Moreover, rather than passively delivering drugs to a site, a more selective strategy involves actively targeting the sites by releasing the drug payload near or inside the affected

Received: March 7, 2025
Revised: May 12, 2025
Accepted: May 16, 2025
Published: June 1, 2025

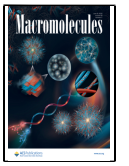

cells. In this regard, polymeric micelles offer a variety of possibilities. For example, by introducing stimuli-responsive functional groups or monomers, it is possible to induce the release of a drug at a specific site using triggers such as light, temperature, or pH.[25] Lastly, decorating micelles with specific moieties, such as ligands, enables targeting of desired sites that have specific receptors for said ligand[26,27] thereby minimizing the contact with healthy cells. Thus, polymeric micelles that serve as drug delivery vehicles should combine a variety of attributes. Fortunately, the vast array of synthetic protocols[28] has made it possible to construct a variety of exotic polymers. One such class that combines multiple benefits and has attracted considerable interest in recent years is linear dendritic block copolymers (LDBCs). These polymers consist of a linear solvophobic block and a precise branched structure consisting of hydrophilic blocks, resembling a tree.[29−31] In solvent, they self-assemble into an even greater variety of structures than linear block copolymers.[32,33] Additionally, LDBCs offer several other advantages over linear block copolymers, including smaller micelle sizes, lower aggregation numbers, and a greater number of chain ends available for functionalization.[34] However, synthesizing LDBCs with a precise branch structure—i.e., with controlled macromolecular weight and branch generations—requires a multipot process.[35,36] This complexity results in relatively high production costs compared to simpler copolymers. An alternative approach which has gained popularity in recent years is to use their less precise cousins, the so-called linear hyperbranched block copolymers (LHBCs).[37,38] In contrast to the case of LDBCs, the branched component of LHBCs is highly random. This randomness arises from their synthetic protocols, which are both blessings and a curse. For example, LHBCs can be synthesized in a one-pot process,[39] considerably reducing production complexity. However, this simplification often comes at the cost of high macromolecular weight and topological polydispersity.[40,41] As drug delivery vehicles must be monodisperse in size and exhibit similar physiological characteristics between batches, it is important for the polymers to form well-defined structures.[42] High macromolecular weight polydispersity can lead to undesirable assemblies.[43] To address this issue, methods that reduce polydispersity, such as slow-monomer addition,[44] have been developed. It should be noted that a certain low degree of macromolecular weight polydispersity may have a positive effect on micelle size uniformity, as has been demonstrated for linear block copolymers.[45] Theoretical studies on micelle formation have mostly focused on monodisperse linear block copolymers[46−51] and LDBCs.[34,52−54] A few simulation studies have investigated micelle self-assembly and morphological transitions in solutions of hyperbranched copolymers with irregular architectures;[55−58] however, the systems were still monodisperse in the sense that all molecules were identical. Only few studies have considered effects of molecular weight polydispersity,[45,59−63] and the effects of topological polydispersity remain largely unexplored. Here, we attempt to elucidate some of the properties of micelles composed of polydisperse LHBCs, and we compare them with their counterparts made of monodisperse linear diblock copolymers and LDBCs. Schematic pictures of such polymers are shown in Figure 1b-e. In the case of LDBCs, the solvophobic blocks comprising the dendritic part have the same total number of monomers, and the number of terminal ends doubles with each generation. We investigate a range of metrics, such as the morphologies of the micelles, the terminal end distributions, the stability of micelles, their CMC values, and their encapsulation capacities for a model solvophobic drug molecule. We also investigated the limiting molecular weight polydispersity that can still be tolerated. To this end, we employ molecular dynamics (MD) simulations to model the slow-monomer addition method[44,64,65] and construct a variety of LHBCs with predetermined macromolecular length (weight) polydispersity. The molecular architectures are then extracted and the self-assembly of the molecules is evaluated in the grand canonical ensemble using the Self-Consistent Field Theory (SCFT) framework.[66]

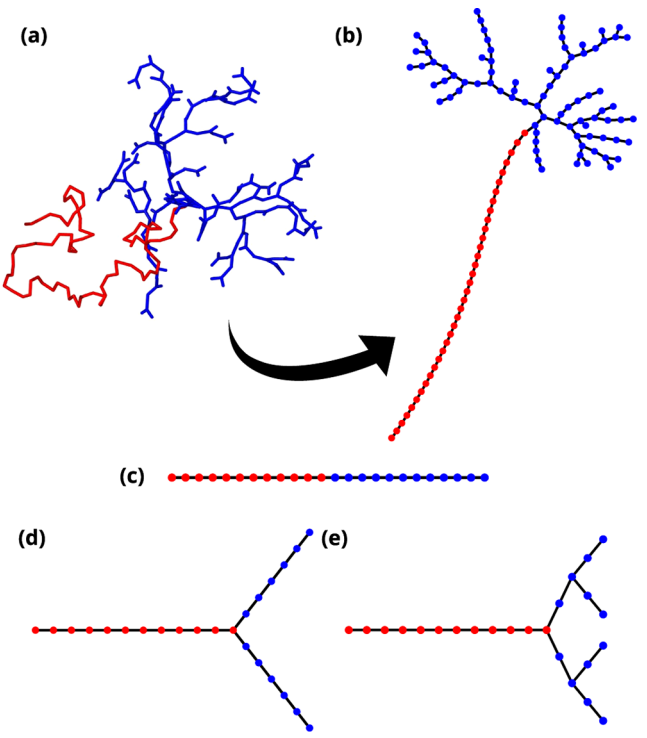

Figure 1. Examples of molecular structures. Solvophobic part is shown in red and solvophilic part in blue. (a) Example of an LHBC molecule produced from a molecular dynamics simulation (see Section 2.1). (b) Graph representation of the polymer molecule in (a) where each filled circle represents a monomer. Note that the maximum number of generations in this particular example is 10. (c) Representation of a symmetric linear diblock molecule. (d, e) Representation of a LDBC molecule of generation one (d) and generation two (e).

2. MODEL AND METHODS

2.1. Molecular Dynamics Model. We employed MD simulations to mimic the slow-monomer addition protocol[67] and used beads labeled A to F to represent various components of the LHBC. Beads F and C represent polystyrene and the macroinitiator, respectively, while the rest are used to represent the AB_2 monomers and are configured in a star-like fashion as shown in Figure 2. The center bead of the star (type D) is connected to two beads B and one bead A such that the four of them form a Y-shape, and further inert beads E are added to stabilize this structure. Beads A can interact via an attractive potential with beads C and B, simulating the irreversible conjugation of AB_2 monomers with the macroinitiator and with each other.

The detailed interactions between each bead type are outlined below:

$$U_{ij}^{\text{harm.}} = \frac{1}{2}k_h(r_{ij} - r_o)^2$$

for bonded beads , F−F, F−C, C−C, A−D, B−D, D−E, (1)

https://doi.org/10.1021/acs.macromol.5c00615
Macromolecules 2025, 58, 5872−5882

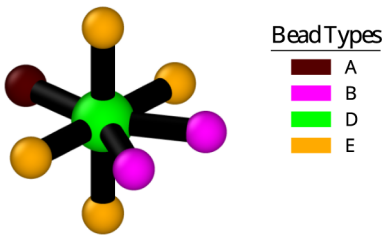

Figure 2. Sketch of the AB_2 monomer used in the MD simulations. Each color corresponds to a different type of bead as indicated, and bonds are depicted in black. In the SCFT calculations, this whole monomer is turned into a single solvophilic segment.

$$U_{ij}^{\mathrm{LJ}} = 4\epsilon\left[\left(\frac{\sigma}{r_{ij}}\right)^{12} - \left(\frac{\sigma}{r_{ij}}\right)^{6}\right]$$

for all bead pairs except , A−C, A−B, (2)

$$U_{ij}^{\mathrm{bind.}} = -d\cos\left(\frac{r_{ij}\pi}{2r_c}\right)\Theta(r_c - r_{ij})$$

for bead pairs, A−C, A−B, (3)

$$U_{ijk}^{\cos} = \frac{1}{2}k_c(\cos(\theta_{ijk}) - \cos(\theta_o))^2$$

for bonded bead triplets , A−D−B, B−D−B, (4)

$$U_{ijkl}^{\mathrm{dihedral}} = \frac{1}{2}k_d(1 - \cos(2\phi_{ijkl}))^2$$

for beads E−E−E−E in the same star unit. (5)

Here r_{ij} denotes the distance between beads i and j, θ_{ijk} is the angle between particles i, j, and k, ϕ_{ijkl} is the angle between the two planes formed by beads i, j, k and beads j, k, l, respectively, and Θ refers to the Heaviside function ($\Theta(x) = 1$ for $x > 0$, $\Theta(x) = 0$ otherwise). The parameters are $\kappa_h = 100\epsilon$, $\rho_o = \sigma$, $d = 100\epsilon$, $r_c = \sigma/2$, $\kappa_c = 100\epsilon$, and $\theta_o = 5\pi/6$ for A-D-B and $\theta_o = 2\pi/3$ for B-D-B.

We simulated the aforementioned system under constant temperature and volume conditions using Langevin dynamics as implemented in the HOOMD-blue molecular dynamics package.[68] Starting with a linear chain of 84 F-beads followed by 8 C-beads connected in a sequential arrangement, we then introduced a designated number of AB_2 monomers. This number is sampled randomly from a Schulz−Zimm distribution[69] with an average value of $\bar{N}_{AB_2} = 76$ monomers, and varying, but prescribed polydispersity index PDI = $\overline{N_{AB_2}^2}/\bar{N}_{AB_2}^2$. We note that the choice of $\bar{N}_{AB_2} = 76$ is based on the fact that in SCF, F beads act as solvophobic monomers, while C beads and AB_2 monomers act as identical solvophilic monomers, thus the resulting LHBCs are, on average, symmetric in terms of the solvophobic-to-solvophilic monomer ratio. For the case of PDI = 1, the ensemble generated consists of LHBCs that are monodisperse in length yet display a diversity of topologies.

The AB_2 monomers are added sequentially, with the condition that the preceding monomer must first be attached to the growing central molecule before a new monomer can be introduced. This prevents premature connections between free AB_2 monomers. A schematic representation of such a polymer molecule and its graph structure is shown in Figure 1a,b. The graph representation of this molecule, along with others that constitute the polydisperse ensemble of LHBCs, is subsequently recorded and used for further calculations within the SCF framework. To avoid confusion, we note that, although more than two types of MD monomers are introduced in the construction of the LHBC polymers, the MD monomers are then mapped onto only two types of segments, either solvophobic or solvophilic, in the SCFT model.

The SCF calculations are done in batches B1−B4, consisting of 128 different polymers each, which are a result of the "greedy algorithm". This algorithm sorts the 512 polymers, which we refer to as the BA batch, into four equally sized sub-batches (B1−B4). It does this by progressively filling these sub-batches while tracking the total sum of monomers in each batch. It then assigns the next polymer to the sub-batch with the lowest total, ensuring that no sub-batch exceeds the target of 128 polymers. More details about the SCF simulations are provided in Section 2.2.

2.2. SCFT Model. To model a system of copolymers with solvophobic (H) and solvophilic (P) monomers in solvent (S), capable of exchanging polymer chains with its environment (bath), we employ SCFT calculations in the grand canonical ensemble.

We consider a polymer solution in implicit solvent, modeled according to the Sanchez−Lacombe theory[66,70] and characterize the system in terms of spatially varying monomer volume fractions $\phi_H(\boldsymbol{r})$ and $\phi_P(\boldsymbol{r})$ that depend on the corresponding monomer number densities $\rho_\alpha(\boldsymbol{r})$ and the monomeric volumes $v_\alpha = v_P$ via $\phi_\alpha = \rho_\alpha v_\alpha$. Thus, the solvent volume fraction is given by $\phi_S(\boldsymbol{r}) = 1 - \phi_H(\boldsymbol{r}) - \phi_P(\boldsymbol{r})$ and the solvent number density is given by $\rho_S = \phi_S/v_S$, where v_S is the volume of a solvent molecule. The grand canonical free energy is given by[66]

$$\begin{aligned}\beta F_{\mathrm{GC}} &= \left(U_{\mathrm{inter.}} - \tfrac{1}{v^*}\int \mathrm{d}\boldsymbol{r}\sum_\alpha^{H,P}(\rho_\alpha v^*)W_\alpha - \sum_i^{n_T}\exp(\beta\mu_i)Q_i\right)\\ U_{\mathrm{inter.}} &= \tfrac{1}{v^*}\Big(\int \mathrm{d}\boldsymbol{r}\sum_\alpha^{H,P}\chi_{\alpha S}\phi_\alpha(\boldsymbol{r})\phi_S(\boldsymbol{r}) + \tfrac{1}{2}\sum_{\alpha,\beta}^{H,P}\chi_{\alpha\beta}\phi_\alpha(\boldsymbol{r})\phi_\beta(\boldsymbol{r})\\ &\quad + v^*(\rho_S(\boldsymbol{r})\ln(\phi_S(\boldsymbol{r})) - \rho_S(\boldsymbol{r}))\Big)\end{aligned} \quad (6)$$

where v* is a reference volume, $U_{\mathrm{inter.}}$ is the interaction potential which also includes the translational entropy of the solvent molecules, $\chi_{\alpha\beta}$ are the Flory−Huggins parameters between species α and β, W_α are the self-consistent fields, μ_i and Q_i is the chemical potential and the single chain partition functions of chains of type i, respectively, n_T is the number of different types of polymers, and V is the volume of the system.

In these grand canonical SCF calculations, we assume the polymers in the micelle to be in chemical equilibrium with a homogeneous solution of chains of type i with global average polymer volume fraction $\bar{\phi}$. The chemical potentials μ_i are then given by

$$\exp(\beta\mu_i + \ln(\bar{N})) = \frac{w_i\bar{\phi}V}{\bar{Q}_i v_P} \quad (7)$$

where $\bar{Q}_i$ is the single chain partition function of chain type i in the homogeneous state and w_i is the fraction of chains of type i in the bath such that $\sum_i^{n_T} w_i = 1$. Also, $\bar{N} = \sum_i^{n_T} w_i N_i$ is the average chain length and N_i is the length of polymer type i. The derivation of eq 7 is given in Appendix A.

In our study, we consider copolymers that are separated into blocks, each consisting exclusively of either solvophobic or solvophilic monomers. We categorize the blocks into three groups based on their connectivity: (1) Stem (SM, one per molecule), (2) Internal (IL), and (3) Terminal (TL). Stem and terminal blocks each have one free end, while internal blocks have none. Blocks are delimited by junctions, which encompass both the internal branch points and free ends. For each molecule type i, the junctions are numbered consecutively, starting from zero, which is assigned to the free end of the stem block. Thus, a given block in a chain of type i can be identified by the pair $[j_1 j_2]_i$ of confining junctions. Moreover, we assign orientations to molecules, defining the forward direction as running from the stem to the terminal blocks. An example illustrating the nomenclature is given in Figure 3.

For each block $[j_1 j_2]_i$, we calculate a forward propagator $q_{[j_1 j_2]_i}(\boldsymbol{r}, s)$ and a backward propagator $q^\dagger_{[j_1 j_2]_i}(\boldsymbol{r}, s)$, where $s = n/\bar{N}$ and n is a monomer count. This is done by solving the modified diffusion equations[71]

https://doi.org/10.1021/acs.macromol.5c00615
Macromolecules 2025, 58, 5872−5882

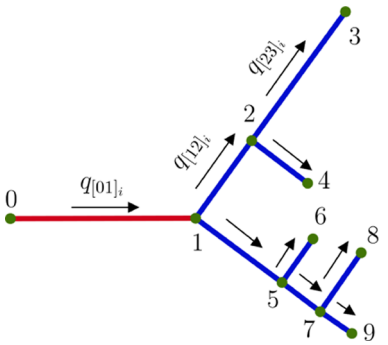

Figure 3. Cartoon representation of a hyperbranched polymer indexed to *i*. Red indicates that block *j* is solvophobic, while blue indicates that the block is solvophilic. Green indicates the junction points numbered here from 0 to 9. For clarity, only some of the forward propagators are shown.

$$\frac{\partial q_{[j_1j_2]_i}(\boldsymbol{r},s)}{\partial s} = \left(\bar{N}\frac{b^2}{6}\nabla^2 - \bar{N}W_{[j_1j_2]_i}(\boldsymbol{r})\right)q_{[j_1j_2]_i}(\boldsymbol{r},s)$$
$$\frac{\partial q^{\dagger}_{[j_1j_2]_i}(\boldsymbol{r},s)}{\partial s} = -\left(\bar{N}\frac{b^2}{6}\nabla^2 - \bar{N}W_{[j_1j_2]_i}(\boldsymbol{r})\right)q^{\dagger}_{[j_1j_2]_i}(\boldsymbol{r},s) \quad (8)$$

where we assumed the statistical segment length of the monomers b to be the same throughout the polymer. Here, $W_{[j_1j_2]_i}$ is either W_H or W_P, depending on the monomer type of block $[j_1j_2]_i$. eq 9 is solved for values of s in the interval $s \in [0, s^{\max}_{[j_1j_2]_i}]$, where $\bar{N}s^{\max}_{[j_1j_2]_i}$ is the macromolecular length of block $[j_1j_2]_i$, with initial conditions given by the following relations:[71]

$$q_{[j_1j_2]_i}(\boldsymbol{r},0) = 1 \text{ for } [j_1j_2]_i = [01]_i \in \text{SM} \quad (9)$$

$$q_{[j_1j_2]_i}(\boldsymbol{r},0) = q_{[j_3j_1]_i}(\boldsymbol{r}, s^{\max}_{[j_3j_1]_i})q^{\dagger}_{[j_1j_4]_i}(\boldsymbol{r},0)$$
$$\text{for } [j_1j_2]_i \notin \text{SM and,}$$
$$[j_3j_1]_i \in \text{SM or IL, } [j_1j_4]_i \in \text{IL or TL} \quad (10)$$

$$q^{\dagger}_{[j_1j_2]_i}(\boldsymbol{r}, s^{\max}_{[j_1j_2]_i}) = 1 \text{ for } [j_1j_2]_i \in \text{TL} \quad (11)$$

$$q^{\dagger}_{[j_1j_2]_i}(\boldsymbol{r}, s^{\max}_{[j_1j_2]_i}) = q^{\dagger}_{[j_2j_3]_i}(\boldsymbol{r},0)q^{\dagger}_{[j_2j_4]_i}(\boldsymbol{r},0)$$
$$\text{for } [j_1j_2]_i \notin \text{TL, } [j_2j_3]_i, [j_2j_4]_i \in \text{IL or TL.} \quad (12)$$

Equations 9 and 11 are the initial conditions for the free ends of the polymer, while eqs 10 and 12 are the initial conditions for the inner junction points of the polymer. For example, in Figure 3, junction points 1, 2, 5, and 7 are inner junction points while the rest are free ends. Based on these initial conditions, we first calculate the backward propagators of the chain, starting from the terminal groups and proceeding "backward" along the chain, up until the stem's backward propagator is calculated. Then, we repeat the procedure for the forward propagator in the reverse order. Once the propagators have been calculated, the volume fractions can be determined via the following expression:

$$\phi_\alpha(\boldsymbol{r}) = \sum_i^{n_T}\phi_{\alpha,i}(\boldsymbol{r}) = \sum_i^{n_T}\exp(\beta\mu_i + \ln(\bar{N}))$$
$$\times\sum_{[j_1j_2]_i}\int_0^{s^{\max}_{[j_1j_2]_i}} \mathrm{d}s\; q_{[j_1j_2]_i}(\boldsymbol{r},s)q^{\dagger}_{[j_1j_2]_i}(\boldsymbol{r},s)\theta_{\alpha,[j_1j_2]_i}, \quad (13)$$

where $\phi_{\alpha,i}(\boldsymbol{r})$ is the volume fraction contribution from chain i to monomer type α and $\theta_{\alpha,[j_1j_2]_i}$ is one if the block $[j_1j_2]_i$ is of type α, and zero otherwise. The single chain partition function of a chain of type i can be evaluated from the backward propagators of the corresponding stem blocks,

$$Q_i = \int \mathrm{d}\boldsymbol{r} q^{\dagger}_{[01]_i}(\boldsymbol{r},0) \quad (14)$$

Finally, to close the self-consistent loop, the fields $W_\alpha(\boldsymbol{r})$ are calculated from the functional derivatives of $U_{\text{inter.}}$ with respect to the monomeric *number* densities[66] $\rho_\alpha = \phi_\alpha/v_\alpha$, as

$$W_\alpha(\boldsymbol{r}) = \frac{\delta U_{\text{inter.}}[\phi]}{\delta\rho_\alpha(\boldsymbol{r})}$$
$$= \frac{v_\alpha}{v^*}\left(\chi_{\alpha S}\phi_S + \sum_\beta^{H,P}(\chi_{\alpha\beta} - \chi_{\beta S})\phi_\beta - \frac{v^*}{v_S}\ln(\phi_S)\right) \quad (15)$$

Given an initial field W_α, we solve eq 9, calculate new volume fractions using eq 13, calculate new fields using eq 15, mix the new fields with the old ones using lambda mixing,[72] and repeat the loop until the following convergence criterion is reached:

$$\text{CF} = \sum_\alpha^{H,P}\int \mathrm{d}\boldsymbol{r}(\phi_\alpha^{\text{new}} - \phi_\alpha^{\text{old}})^2 < 10^{-12} \quad (16)$$

All SCF calculations were performed with periodic boundary conditions in a simulation box of volume $V = 15 \times 15 \times 15\ [\bar{R}_g^3]$, using 1024, 128×128, and $64 \times 64 \times 64$ grid points for one-, two-, and three-dimensional simulations, respectively. The rest of the parameters were chosen as $\chi_{HP}\bar{N} = 30$, $\chi_{HS}\bar{N} = 61$, $\chi_{PS}\bar{N} = 27$, $v_S/(v^*\bar{N}) = 0.02$, and $v^* = v_P$ such that the equilibrium morphology in a system of symmetric diblock copolymers is a spherical micelle. To accelerate the numerical computation of the propagators for highly symmetric architectures like LDBCs, we implemented schemes similar to those in Yong and Kim,[73] which avoid redundant calculations of identical propagators.

3. RESULTS AND DISCUSSION

In this section, we first examine the results related to the size and topological polydispersity of LHBCs generated from MD simulations. We then present results from SCF calculations, comparing micelles formed by polydisperse ensembles of LHBCs with those formed by monodisperse ensembles of linear diblocks or LDBCs of various generations. Key experimentally relevant quantities such as the critical micelle concentrations (CMC), the equilibrium morphologies, the volume fraction profiles, the terminal end distributions, the number of chains n_M and terminal ends c_M per micelle, the micelle size distributions, and the energy penalty associated with asphericity are discussed. Finally, we investigate the drug encapsulation capacity of these micelles by evaluating the encapsulation of solvophobic homopolymers. For a fair comparison, we limit the study to systems with solvophobic-to-solvophilic monomer ratio maintained at 1:1 for all monodisperse LDBC and linear diblock systems, and on average, at 1:1 for the polydisperse LHBC systems. We note that, in some of the following plots, we refer to the linear diblock chain as zeroth generation LDBC. Below, lengths are mostly given in units of the average radius of gyration $\bar{R}_g = b\sqrt{\bar{N}/6}$ and the free energy F will be given in units of $k_B\,T = \beta^{-1}$ and rescaled with the Ginzburg parameter $\bar{C} = \bar{R}_g^3/v^*\bar{N}$.

3.1. Generation of Representative LHBC Polymer Sets.

As noted in the introduction, slow monomer addition can yield polymers with low macromolecular length polydispersity, which shows particular promise for applications. Therefore, we focus on LHBCs synthesized by using this approach. Specifically, we modeled the slow-monomer addition protocol outlined in Barriau et al.[44] In this process, a linear polystyrene block is initially conjugated to a short linear hydroxylated polybutadiene

https://doi.org/10.1021/acs.macromol.5c00615
Macromolecules 2025, 58, 5872−5882

block, which serves as a macroinitiator for the subsequent gradual addition of glycidol, ultimately forming the LHBC molecule. Here, glycerol acts as an AB_2-type monomer, thus the branching points in the resulting hyperbranched polyglycerol have a degree of three.

To model the slow monomer addition protocol, we used single-chain coarse-grained MD simulations. In such simulations, a linear block was conjugated to a linear macroinitiator and a predetermined number of AB_2 monomers, that can irreversibly bond with the macroinitiator and other AB_2 monomers, were added sequentially to the growing molecule. This predetermined random number followed a Schulz−Zimm distribution with a specific polydispersity index (PDI) and average number (Section 2.1).

We investigated different values of PDI, and for each PDI, we simulated the creation of 512 independent polymers. To keep the SCF simulations manageable and enable assessing statistical errors in the SCF results, we divided the complete batch (BA) into four subbatches (B1, B2, B3, B4) of 128 polymers each. Instead of randomly selecting polymers from the BA batch, we used a "greedy number partitioning" algorithm to assign polymers to sub-batches (see Section 2.1).

This method ensures that the four sub-batches have similar average chain lengths and was also found to preserve other key characteristics. For instance, the degree of branching[74] which is defined as

$$\mathrm{DB} = 2D/(2D + L) \tag{17}$$

where D and L are the number of dendritic monomers (branching points) and linear monomers, is also preserved along with the length polydispersity. This is illustrated in both Figure 4 and Table 1, which demonstrate that the characteristics of both the topological and chain length polydispersity are overall inherited from the large BA batch in the sub-batches B1−B4. Note that as explained in Section 2.1, the macroinitiator and the AB_2 monomers are considered solvophilic and compose the entire hyperbranched part of the polymer. The results are consistent with previous Monte Carlo simulations.[75]

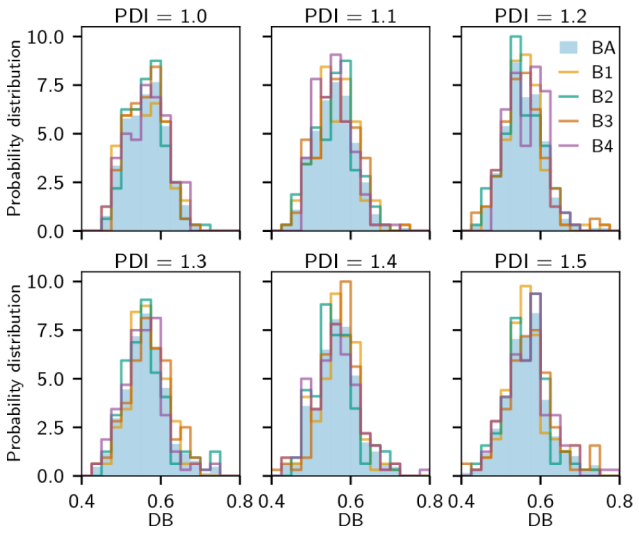

Figure 4. Probability distributions of the degree of branching (DB) for the LHBCs with different values of polydispersity index PDI. The whole colored distribution represents the complete batch (BA), while the other four colors represent the sub-batches (B1−B4). Note that the DB values are calculated only for the solvophilic part of the polymer.

3.2. Equilibrium Micelle Structures. To determine the equilibrium morphology and the CMC of the systems, we conducted one-, two-, and three-dimensional SCF calculations in the grand canonical ensemble, which resulted in lamellae, cylindrical, or spherical micelles, respectively. For simplicity, we only consider solvophobic (H), solvophilic (P), and solvent (S) in these calculations and do not distinguish between the macroinitiator and the AB_2 monomers, to which we all refer as P. In particular, we assume that all monomers have the same monomeric volume v_P. We further assume that the polymers in the micelle are in chemical equilibrium with a homogeneous solution (bath) of chains of type i with global average polymer volume fraction $\overline{\phi}$. The chemical potentials μ_i (eq 7) of each type are then given in terms of w_i, which is the fraction of chains of type i in the bath. We set $w_i = 1/n_T$, meaning that chains of all types i are incorporated into the micelle with the same *a priori* probability. The actual fraction of chains i in the micelle may of course differ from w_i.

First, we varied the average polymer volume fraction, $\overline{\phi}$, of the bath and evaluated the free energy difference (ΔF) between the inhomogeneous and homogeneous states for each case. Selected curves for ΔF as a function of $\overline{\phi}$ are shown in Figure 5a,b. The critical volume fraction, $\overline{\phi}_c$, is defined as the lowest value of $\overline{\phi}$ among the three morphologies for which $\Delta F = 0$. This represents the lowest polymer volume fraction at which micelles begin to form, with the corresponding morphology being the equilibrium micelle morphology. The resulting values of $\overline{\phi}_c$ and the respective morphologies are shown in the insets of Figure 5: as a function of PDI for LHBCs in Figure 5a, and as a function of generations for LDBCs in Figure 5b. In LDBC systems, $\overline{\phi}_c$ increases with increasing generations, consistent with prior findings.[34] In LHBC systems, $\overline{\phi}_c$ decreases with increasing PDI, which aligns with observations from micelles formed by linear block copolymers with a polydisperse solvophilic block.[45] For all polymer systems tested, the equilibrium morphology was spherical micelles, except for LHBCs at PDI = 1.5, which transitioned to cylindrical micelles. In Figure 5c, the differences in the length distribution of the solvophilic part between the micelle and bath are shown for the different LHBC systems. Greater polydispersity results in a larger proportion of both smaller and larger chains in the bath. Smaller chains, being overall more solvophobic, are preferentially attracted to the micelle, while larger chains are preferred in the bath. Additionally, chains with smaller solvophilic parts lose less configurational entropy upon incorporation into micelles compared to larger chains, which explains the decrease in $\overline{\phi}_c$ with increasing PDI. The eventual transition of the equilibrium morphology from spherical to cylindrical can be attributed to smaller chains having a higher packing parameter.[76] Figure 5d demonstrates that the effects of topology are minimal as the differences in the degree of branching within the micelle and the bath for the PDI = 1 case are negligible. At PDI = 1, all chains have equal molecular weight, so there is no size-based driving force, unlike in the other cases. Thus, the differences observed for the other PDI cases can be primarily attributed to indirect effects of molecular weight polydispersity, rather than topological polydispersity. However, this does not rule out a potential impact of topological polydispersity in systems with fewer chains than those tested.

Next, we compare the properties of the equilibrated spherical micelles. We define the terminal end distribution $c(r)$, the number of chains n_M, and the number of terminal ends in the micelle, c_M, as

https://doi.org/10.1021/acs.macromol.5c00615
Macromolecules 2025, 58, 5872−5882

Table 1. Statistical Properties of Polymers in Each Representative Batch of LHBC Molecules (See Text), with Notation "Average Number of AB_2 Monomers"("PDI")/"DB ± Error of DB"[a]

Target PDI	1.0	1.1	1.2	1.3	1.4	1.5
BA	76.0(1.00)/0.56±0.05	76.1(1.10)/0.56±0.05	74.3(1.18)/0.56±0.05	75.6(1.33)/0.57±0.05	73.4(1.37)/0.57±0.05	74.7(1.56)/0.57±0.06
B1	76.0(1.00)/0.56±0.05	76.1(1.10)/0.56±0.05	74.3(1.18)/0.56±0.05	75.6(1.34)/0.57±0.05	73.5(1.37)/0.57±0.05	74.7(1.56)/0.57±0.06
B2	76.0(1.00)/0.56±0.04	76.2(1.10)/0.56±0.05	74.3(1.18)/0.56±0.05	75.6(1.33)/0.57±0.06	73.4(1.37)/0.56±0.05	74.7(1.56)/0.56±0.05
B3	76.0(1.00)/0.56±0.04	76.2(1.10)/0.56±0.05	74.3(1.18)/0.56±0.05	75.6(1.33)/0.57±0.05	73.4(1.37)/0.57±0.05	74.7(1.55)/0.57±0.06
B4	76.0(1.00)/0.56±0.05	76.0(1.10)/0.56±0.05	74.3(1.18)/0.56±0.05	75.6(1.32)/0.56±0.06	73.4(1.37)/0.56±0.06	74.7(1.55)/0.57±0.06

[a]Note that the calculation of DB involves only the solvophilic part of the polymer, while the calculation of the PDI involves only the AB_2 monomers. Small deviations from the target values arise due to sampling.

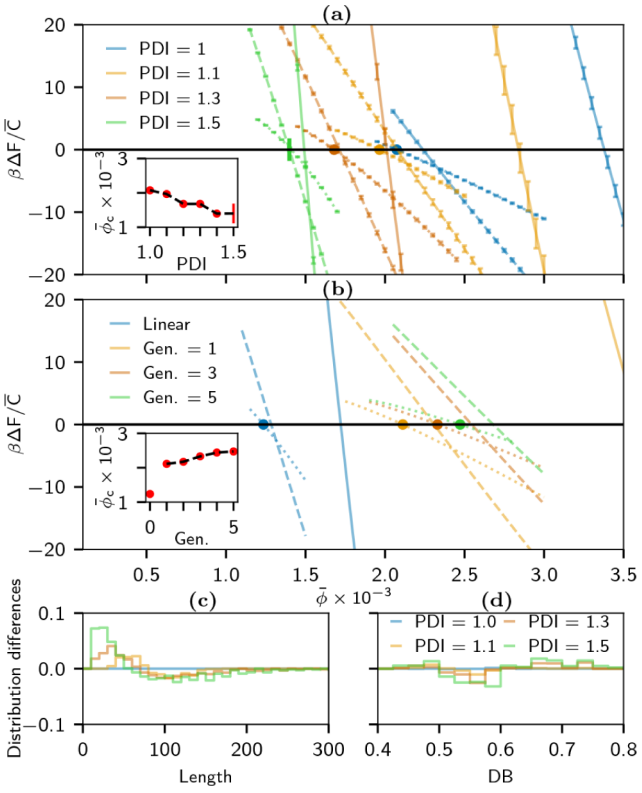

Figure 5. (a,b): Rescaled free energy difference ΔF between homogeneous and inhomogeneous states against the average polymer volume fraction in the bath $\bar{\phi}$ for polydisperse LHBCs (a) and monodisperse linear and LDBCs (b). Each color corresponds to a different polymer system, while the style of the line corresponds to lamella (solid line), cylindrical (dashed line), and spherical (dotted line) micelle states. For LHBCs (a), errors obtained from averaging over batches are also shown. The insets in (a) and (b) show the state with the lowest critical concentration $\bar{\phi}_c$ against PDI and number of generations, respectively. The circular (●) and rectangular (■) symbols represent spherical micelles and cylindrical micelles, respectively, as the equilibrium morphology, in both the main and inset plots. (c,d): Differences in the distribution of chain lengths and degree of branching between the bath and micelle were observed for LHBCs. The macromolecular weight and DB are calculated only for the hyperbranched part of the LHBCs.

$$c(\boldsymbol{r}) = \sum_{i}^{n_T} \exp(\beta\mu_i + \ln(\bar{N})) \times \sum_{[j_1 j_2]_i}^{TL} q_{[j_1 j_2]_i}(\boldsymbol{r}, s^{\max}_{[j_1 j_2]_i}) q^{\dagger}_{[j_1 j_2]_i}(\boldsymbol{r}, s^{\max}_{[j_1 j_2]_i}) \tag{18}$$

$$c_M = \int_{V_c} \mathrm{d}V\ c(\boldsymbol{r})/v_P \tag{19}$$

$$n_M = \int_{V_c} \mathrm{d}V\ \phi_H(\boldsymbol{r})/(N_H v_P) \tag{20}$$

where the sum is performed over the terminal blocks (TL) of chain type i, V_c is a sphere with a cutoff radius of 6.0 $[\bar{R}_g]$ and N_H is the length of the solvophobic block. The solvophobic volume fraction ϕ_H, the backward propagator q and $q^{\dagger}$, as well as the notation are defined in Section 2.2. In Figure 6a, the volume

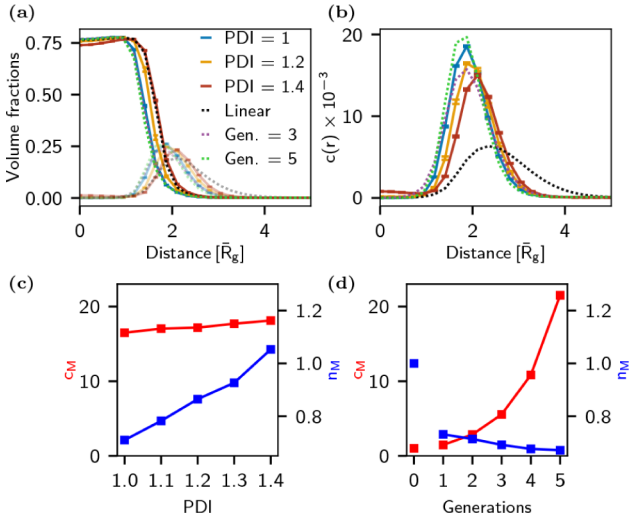

Figure 6. (a) Volume fraction profiles for spherical micelles at their CMC vs the distance from the center. The opaque lines correspond to the solvophobic monomers while the translucent lines correspond to the solvophilic monomers. (b) Normalized average chain end profiles vs the distance from the center of the micelles. The colors and line style for each polymer system are shown in the legend. For the LHBC systems, errors are also shown. (c, d): Number of solvophilic chain ends in the micelle c_M (red) and number of chains in the micelle n_M (blue) normalized by the corresponding number for monodisperse linear diblock chains for LHBCs as a function of PDI (c) and LDBCs as a function of generation number (d).

fraction profiles of equilibrium micelles are shown for a selection of polymer systems. These profiles are only marginally influenced by polydispersity, with the LHBC systems exhibiting profiles that lie between those of the linear and the other LDBC-based micelle systems. The results indicate that the impact of polydispersity on the equilibrium volume fraction profiles is relatively minor compared to other factors, such as polymer architecture or the generation of LDBCs. These findings are consistent with a previous study on micelles formed by linear block copolymers[45] which showed that polydispersity in the

https://doi.org/10.1021/acs.macromol.5c00615
Macromolecules 2025, 58, 5872−5882

solvophobic block had a strong effect on the volume fraction profiles, whereas polydispersity in the solvophilic block had little to no effect. We note that the solvent content in the micelle core is relatively high in these calculations, around 25%. This is a consequence of the monomer−solvent interactions ($\chi_{HS} = 0.61$) being relatively small. This value is inspired by an empirical estimate for polystyrene in *n*-decane based on Hansen's solubility parameters.[77] The χ_{HS} values for hydrophobic components of pharmaceutical micelles in water, such as polylactate, are typically about twice as high; therefore, the solvent content in the micelle core will be lower. However, this should not change the general trends.

An interesting effect is observed in the high PDI case (PDI = 1.4). As shown in Figure 6a,b, a sizable amount of solvophilic monomers enters the predominantly solvophobic core, leading to a corresponding decrease in the solvophobic contribution. High PDIs can result in polymers with small solvophilic contributions, which makes them nearly entirely solvophobic. Consequently, the polymers tend to position themselves deeper within the micelle core. As a result, polymers with small solvophilic blocks may occasionally flip with their solvophilic segments pointing inward rather than outward. This flipping behavior explains the reduced solvophobicity and the slight increase of the solvophilic contributions within the core. It highlights the complex nature of micelle formation at high polydispersity, where the distribution of solvophobic and solvophilic monomers becomes less predictable. The phenomenon may also explain the paradoxical observation that the equilibrium micelle size increases with increasing PDI, despite being composed of smaller chains. In other words, the shorter chains, which behave almost entirely as solvophobic molecules, contribute to swelling of the micelle core. When comparing the volume fraction profiles of LHBC and LDBC micelles to those of micelles composed of linear chains, as shown in Figure 6a, one finds that the LHBC micelles at high PDI exhibit the highest resemblance. In contrast, the normalized terminal end distributions in Figure 6b present a different picture. Here, LHBCs show greater similarity to LDBCs than to their linear counterparts, as they feature a much more concentrated corona. Increasing the PDI shifts the peak of the distribution toward larger values, which is consistent with the expected increase in the micelle size. Unexpectedly, the number of terminal ends, c_M, for LHBCs appears to remain relatively constant with respect to PDI, showing only a minute increase as PDI increases, as illustrated in Figure 6c (red curve). This results from the interplay of two opposing factors: As can be seen in Figure 6c (blue curve), the number of chains, n_M, increases with increasing PDI in LHBC micelles, consistent with the increase in the micelle size discussed above. On the other hand, the ratio c_M/n_M, which corresponds to the average number of terminal ends per polymer in the micelle, decreases with PDI due to the preference for shorter chains in such micelles. Therefore, despite larger PDIs leading to larger micelles, which would typically result in a higher c_M, the presence of shorter chains with fewer terminal ends keeps the c_M relatively unchanged. In LDBC micelles, a similar competition arises. The number of terminal ends per chain increases exponentially with increasing number of generations, but the number of chains n_M decreases (see Figure 6d, blue curve). However, in this case, the first effect dominates by far, such that the number of chain ends in LDBC micelles still increases exponentially as a function of the generation number (Figure 6d, red curve), at least up to the fifth generation.

3.3. Micelle Size and Shape Fluctuations. After we discussed the properties of equilibrium micelles, we now turn to the free energy penalties associated with deviations from the preferred micelle size and shape. This analysis gives information on the stability and polydispersity of micelles and on their resistance to deformations. The small statistical errors observed in Figures 5 and 6 for LHBCs indicate that a single sub-batch is sufficient to capture the behavior of the entire ensemble. Therefore, from this point onward, the results for the LHBC ensembles will be based on the B1 batch for each PDI.

We first examine the energy difference $F_M(R_M)$ between the equilibrium spherical micelle and a micelle of radius R_M in a bath with an average polymer volume fraction $\overline{\phi}_c$. To this end, we introduce a constraint potential in eq 21,

$$V_{\mathrm{con}}[\phi_A] = \frac{\kappa_{\mathrm{con}}}{2\nu^*}\left(\int_{V_{\mathrm{ell.}}} \mathrm{d}\boldsymbol{r}\ \phi_H(\boldsymbol{r}) - \phi_{\mathrm{con}} \right)^2 \tag{21}$$

where the integral is performed over an ellipsoid of volume $V_{\mathrm{ell.}}$ concentered with the micelles. We note that the additional energy term from eq 21 is not explicitly added to the free energy $F_M(R_M)$, only the field contribution of this potential is included, as was similarly done in Mantha et al.[45] We define the micelle radius (R_M) as the radius at which $\phi_H = 0.5$, and the radius is calculated post hoc following the SCF calculations.

The results, shown in Figure 7, indicate that the most stable micelles, as characterized by the height of the energy barrier, are

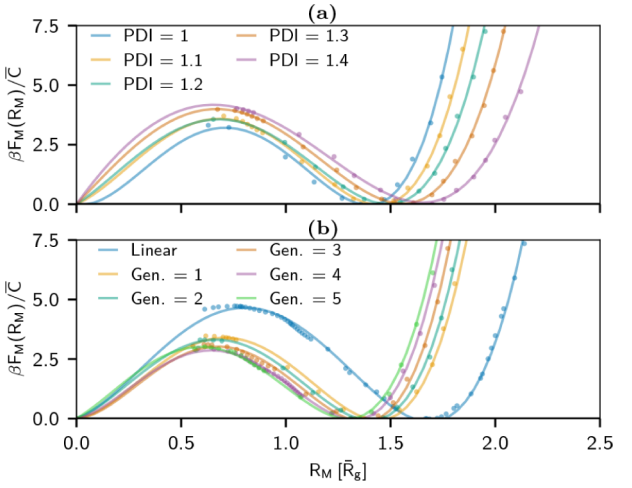

Figure 7. Rescaled free energy of the micelle $F_M(R_M)$ vs the radius of the micelle R_M, for different PDIs (a) or linear and LDBCs (b) at their respective critical volume fractions $\overline{\phi}_c$. The results were obtained by varying ϕ_{con} in the constraint potential of eq 21, while $\kappa_{\mathrm{con}}\overline{N} = 1$ and $V_{\mathrm{ell.}}$ which is a sphere of radius $R/\overline{R}_g = 5$, were kept constant. A fourth-order polynomial was fitted to each system.

those composed of linear polymers, followed by the system with PDI = 1.4. Increasing the PDI leads to a moderate increase in the energy barrier, while, for LDBCs, increasing the number of generations slightly reduces it. Both behaviors can be attributed to the growing and decreasing number of chains within the micelle for increasing PDI and number of generations, respectively.

Furthermore, we can inspect the curvature of $F_M(R_M)$ at the minimum, which is related to the size distribution of micelles *via* $P(R_M) \propto \exp(\beta F(R_M))$. For micelles composed of monodisperse copolymers, the curvature appears to be largely independent of

https://doi.org/10.1021/acs.macromol.5c00615
Macromolecules 2025, 58, 5872−5882

the copolymer architecture. It is very similar for linear copolymers, LDBCs, and LHBCs with PDI = 1. However, if one increases the PDI in the LHBC systems, then the curvature decreases, indicating a broadening of the micelle size distribution. We attribute this to the greater number of smaller chains within the micelles. These smaller chains contribute to the swelling of the micelles and help stabilize a broader range of micelle sizes.

In a similar manner, we investigate the penalty associated with deforming the equilibrium micelles, thus making them aspherical. To define this quantity we consider the normalized moment of inertia tensor, which we define as

$$I_{ij} = \frac{\sum_p \phi_H^{(p)}(|r_{(p)}|^2\delta_{ij} - x_i^{(p)}x_j^{(p)})}{\sum_p \phi_H^{(p)}} \text{ for } i, j = 1, 2, 3 \tag{22}$$

where the sum over p runs over all grid points obeying $\phi_H \geq 0.05$, $x_i^{(p)}$ and $|r_{(p)}|$ are the Cartesian components and the distance from the center of the micelle, respectively. The asphericity of a micelle is then defined as

$$A = \lambda_z^2 - \frac{(\lambda_x^2 + \lambda_y^2)}{2} \tag{23}$$

where $\lambda_{x,y,z}$ are the eigenvalues of the tensor in eq 22.

To impose different asphericities, we again use the constraint potential defined in eq 21. However, since this time we wish to study the response of a given equilibrium micelle to mechanical deformation, we fix the total number of chains in the system, n_b, as well as the chain composition and perform the SCF calculations in the canonical ensemble.

Figure 8 presents the energy penalty for deforming micelles as a function of asphericity in the systems of interest along with two example morphologies depicting the change from a spherical micelle to a cigar like micelle. The figures show that LDBC micelles and LHBC micelles at PDI = 1 case exhibit similar

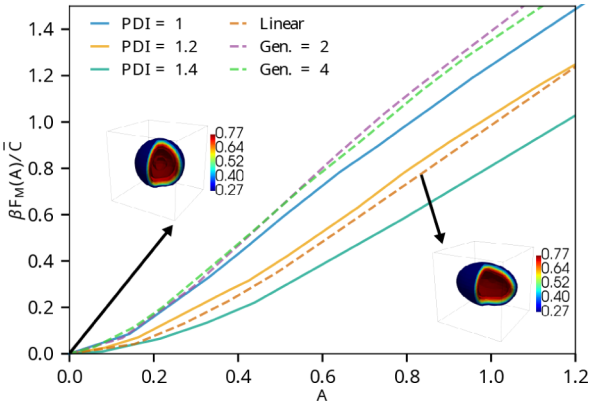

Figure 8. Free energy penalty F_M for deforming a micelle from spherical to aspherical vs asphericity A for LHBC micelles (solid lines) and micelles composed of monodisperse LDBCs and linear copolymers (dashed lines). To enforce different asphericities, the constraint potential of eq 21 was used, with $V_{ell.}$ representing a spheroid with increasing size in the x-direction and decreasing size in the y and z directions such that $V_{ell.}$ matches the volume of the equilibrium micelle core, which was defined as the volume that obeys $\phi_H \geq 0.5$. $\kappa_{con}\bar{N}$ was set to 1 while ϕ_{con} was determined by the volume contribution of the solvophobic micelle core at $A = 0$. Also shown with corresponding arrows are contour plots of the resulting morphology for the linear diblock results at $A = 0$ and $A = 0.84$.

resistance to deformation from their spherical shape, featuring the highest structural stability compared to other, more deformable systems. This is expected, as the topology of LDBCs aligns naturally with spherical micelles, and PDI = 1 polymers, although slightly more flexible, mimic LDBCs. This minor increase in malleability in LHBC micelles at PDI = 1 can be attributed to the diversity of polymer topologies within the micelle, which can arrange themselves in favorable positions so that for a given asphericity a smaller energy penalty is paid. Conversely, increasing the PDI in LHBC systems enhances the structural flexibility of the micelles, making the PDI = 1.4 system even more flexible than the linear micelle.

As the PDI increases, the diversity in chain topology and size also grows. Consequently, chains of different lengths adopt different spatial conformations within the micelle, as shown in Figure S2a,b. The increased diversity enhances adaptability to stress since chains can adjust to micelle deformations by repositioning and reorientating. This is illustrated in Figure S2d which demonstrates that in a stretched micelle, the proportion of long chains oriented along the stretched axis, relative to short chains, is higher along the long axis than along the short axis.

3.4. Encapsulation of Solvophobic Drug Molecules. To conclude our investigation, we analyzed the encapsulation properties of the micelle systems using a solvophobic homopolymer made of type A monomers with a length equivalent to the linear solvophobic segment of each system. We fixed this homopolymer's contribution to the total polymer volume fraction at $\bar{\phi}_h = 10^{-5}$, to maintain consistent encapsulation conditions across all micelle configurations. Simulations were then rerun for each system of interest. The resulting data are presented in Figure 9.

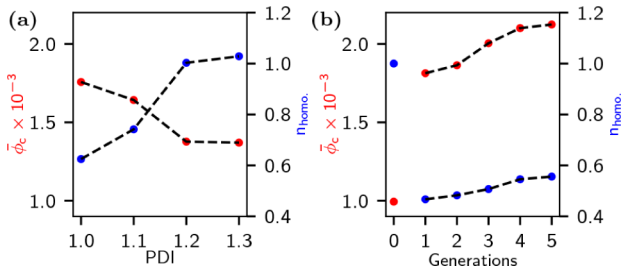

Figure 9. Critical volume fraction $\bar{\phi}_c$ (excluding the contribution from the homopolymers $\bar{\phi}_h$) (red) and average number of homopolymer chains in the simulation box $n_{homo.}$, normalized by the corresponding number for monodisperse linear diblock chain (blue) vs the polydispersity of LHBCs (a) and the number of generations of LDBCs (b). The homopolymer volume fraction in the reservoir solution is kept fixed at $\bar{\phi}_h = 10^{-5}$.

The CMC follows trends similar to those observed without encapsulation; however, CMC values across all systems are lower, a phenomenon commonly reported with the addition of solvophobic drugs.[78] Encapsulation also affects the equilibrium morphology in LHBCs such that they adopt a cylindrical morphology already at PDI = 1.4.

All LHBC systems exhibit superior encapsulation capacities compared with LDBC systems, and increasing PDI further increases this capacity. We attribute this to the fact that, as the homopolymer is incorporated within the micelle, the micelle swells and its size deviates from the equilibrium values in the absence of the drug, as illustrated in Figure S3a. As we noted before, swelling is penalized more strongly in LDBCs compared

https://doi.org/10.1021/acs.macromol.5c00615
Macromolecules 2025, 58, 5872−5882

with LHBCs (Figure 7). Indeed, Figure S3 shows that the micelle core size of LDBCs does not change upon incorporation of the homopolymer. Therefore, LHBCs can accommodate a higher payload due to their flexibility in size fluctuations.

4. CONCLUSION

We investigated self-assembled micelles composed of polymers with a monodisperse linear solvophobic block and a solvophilic block of equal average molecular weight, which are either polydisperse hyperbranched (LHBC), monodisperse dendritic (LDBC), or monodisperse linear (diblock). To do so, we first constructed a set of polydisperse topologies for the hyperbranched case, mimicking the slow-monomer addition synthesis protocol in MD simulations. Subsequently, we continued our investigation using self-consistent field (SCF) numerical calculations. For this purpose, we developed a methodology that incorporates the random branching characteristics of LHBCs and we simulated these systems in the grand canonical ensemble to account for the exchange of polymers between micelles and their environment.

We found that increasing the polydispersity in LHBCs improves the stability of micelles and lowers the critical micelle concentration (CMC). This effect is largely driven by smaller chains that are relatively more solvophobic and therefore exhibit an increased tendency to be incorporated into micelles. In contrast, the topology of the polymers appears to have a smaller impact in these systems, resulting in only slight differences in the aforementioned characteristics compared to LDBC systems.

Volume fraction profiles and terminal end distributions were also found to be broadly similar between the LHBC and LDBC micelles. However, the number of chain ends in LHBC micelles was found to be surprisingly independent of polydispersity and comparable to micelles composed of LDBCs with five generations. This independence is attributed to a combination of two factors: an increase in the number of chains within the micelle with increasing polydispersity and a simultaneous decrease in the average number of terminal ends per chain in the micelle due to the higher content of shorter chains, which naturally have a smaller number of terminal ends.

Our calculations suggest that LHBC micelles are generally more diverse in size and offer less resistance to deformations from their spherical shape compared to that of LDBC micelles. Finally, we probed the capability of the micelles to encapsulate solvophobic drugs by testing them with a solvophobic homopolymer. We found that due to their increased malleability, LHBCs can accommodate a larger payload than LDBCs, although encapsulation can influence their equilibrium morphologies and may induce a transition from spherical to cylindrical morphologies.

In summary, we have demonstrated that LHBC micelles exhibit behaviors similar to those of LDBC micelles, with findings indicating that the random topology of LHBCs is not the primary determinant of their characteristics. The polydispersity in size plays a more significant role. Additionally, the increased diversity in LHBCs proves advantageous, contributing to the enhanced encapsulation capacity and improved stability. We believe, therefore, that the randomness inherent in LHBCs can be thought of not as a drawback but as an attribute that can be explored and taken advantage of.

Future research could explore reverse micelles, where the branched blocks form the core, as in this type of systems, the influence of topology is expected to be more pronounced compared to the systems examined here.[55,79] Additionally, exploring the effects of terminal group modifications on these polymers could further refine our understanding of micelle behavior. We have made our code available as part of the SCF package published in Qiao et al.[80] which can be used to simulate multiblock copolymers of any tree-like graph topology and is parallelized for polydisperse systems.

APPENDIX A

Additional calculations

In homogeneous systems, the fields and propagators do not vary spatially and the propagator equations, eq 9, can be solved analytically. This results in

$$q_{[j_1j_2]_i}(s)q^{\dagger}_{[j_1j_2]_i}(s) \equiv \frac{\bar{Q}_i}{V} \text{ for all } [j_1j_2]_i \text{ and } s$$

and the following expression for the contribution of chain i to the volume fraction of type α:

$$\begin{aligned}\bar{\phi}_{\alpha,i} &= \nu_P \exp(\beta\mu_i + \ln(\bar{N})) \times \sum_{[j_1j_2]_i} \int \mathrm{d}s \\ &\quad q_{[j_1j_2]_i}(s)q^{\dagger}_{[j_1j_2]_i}(s)\theta_{\alpha,[j_1j_2]_i} \\ &= \nu_P \exp(\beta\mu_i + \ln(\bar{N}))\frac{\bar{Q}_i}{V} f_{\alpha,i}\frac{N_i}{\bar{N}}\end{aligned}$$

where $\theta_{\alpha,[j_1j_2]_i}$ is 1 if the block $[j_1j_2]_i$ has the type α and 0 otherwise, the sum $[j_1j_2]_i$ runs over all blocks in the chain i and $f_{\alpha,i}$ is the fraction of chain type i that is of type α. The average volume contribution of the polymer i of monomer type α can also be written as

$$\bar{\phi}_{\alpha,i} = \frac{w_i f_{\alpha,i} N_i}{\bar{N}}\bar{\phi}$$

Equating the two equations above leads to eq 7. We should note that eq 7 remains valid even if $\bar{Q}_i$ is not evaluated in SCF approximation, but by more sophisticated means. Taking into account effects of nonideal chain conformations, *e.g.*, due to the fact that solvophobic blocks of isolated chains might collapse[81] would shift the values of $\bar{Q}_i$ and hence μ_i. Here, we neglect such effects for consistency. In full inhomogeneous SCF calculations, the micelles are also surrounded by a homogeneous solution, and we design the study such that this solution is equivalent to the reservoir solution.

ASSOCIATED CONTENT

Data Availability Statement

The data and code for the MD simulations and SCF calculations can be found at: https://gitlab.rlp.net/mgiannak/hyperbranched.

Supporting Information

The Supporting Information is available free of charge at https://pubs.acs.org/doi/10.1021/acs.macromol.5c00615.

Contains information about chain size distribution in micelles for different sizes (S1), volume fraction profiles for aspherical micelles (S2), change of micelle radius comparison with and without encapsulation of homopolymers (S3), free energy differences against free chain concentration with homopolymers encapsulation (S4), and correlation between order of time of addition and distance against the generation number (S5) (PDF)

https://doi.org/10.1021/acs.macromol.5c00615
Macromolecules 2025, 58, 5872−5882

AUTHOR INFORMATION

Corresponding Authors

Marios Giannakou − *Institut für Physik, Johannes Gutenberg-Universität, Mainz 55099, Germany;* orcid.org/0000-0002-1306-3129; Email: mgiannak@uni-mainz.de

Oleg Borisov − *Institut des Sciences Analytiques et de Physico-Chimie pour l'Environnement et les Matériaux, Pau 64053, France;* orcid.org/0000-0002-9281-9093; Email: oleg.borisov@univ-pau.fr

Friederike Schmid − *Institut für Physik, Johannes Gutenberg-Universität, Mainz 55099, Germany;* orcid.org/0000-0002-5536-6718; Email: friederike.schmid@uni-mainz.de

Complete contact information is available at: https://pubs.acs.org/10.1021/acs.macromol.5c00615

Notes

The authors declare no competing financial interest.

ACKNOWLEDGMENTS

This work was funded by the German Science Foundation (DFG) within grant number 446008821, and the Agence Nationale de La Recherche, France. Partial funding was also received by the DFG within grant number 429613790. M.G. is an associate member of the integrated graduate school of the collaborative research center TRR 146 "Multiscale modeling of soft matter systems", grant number 233630050.

REFERENCES

(1) Hamley, I. W. *The physics of block copolymers*; Oxford University Press, 1998.

(2) Matsen, M. W.; Schick, M. Microphases of a Diblock Copolymer with Conformational Asymmetry. *Macromolecules* **1994**, *27*, 4014−4015.

(3) Khandpur, A. K.; Foerster, S.; Bates, F. S.; Hamley, I. W.; Ryan, A. J.; Bras, W.; Almdal, K.; Mortensen, K. Polyisoprene-Polystyrene Diblock Copolymer Phase Diagram near the Order-Disorder Transition. *Macromolecules* **1995**, *28* (26), 8796−8806.

(4) Mai, Y.; Eisenberg, A. Self-assembly of block copolymers. *Chem. Soc. Rev.* **2012**, *41*, 5969−5985.

(5) Bates, M. W.; Lequieu, J.; Barbon, S. M.; Lewis, R. M.; Delaney, K. T.; Anastasaki, A.; Hawker, C. J.; Fredrickson, G. H.; Bates, C. M. Stability of the A15 phase in diblock copolymer melts. *Proc. Natl. Acad. Sci. U. S. A.* **2019**, *116*, 13194−13199.

(6) Meier, D. J. Theory of block copolymers. I. Domain formation in A-B block copolymers. *J. Polym. Sci. Part C: Polym. Symp.* **1969**, *26*, 81−98.

(7) Ohta, T.; Kawasaki, K. Equilibrium Morphology of Block Copolymer Melts. *Macromolecules* **1986**, *19*, 2621−2632.

(8) Park, M.; Harrison, C.; Chaikin, P. M.; Register, R. A.; Adamson, D. H. Block copolymer lithography: Periodic arrays of holes in 1 square centimeter. *Science* **1997**, *276*, 1401−1404.

(9) Thurn-Albrecht, T.; Derouchey, J.; Russell, T. P.; Jaeger, H. M. Overcoming interfacial interactions with electric fields. *Macromolecules* **2000**, *33*, 3250−3253.

(10) Krausch, G.; Magerle, R. Nanostructured thin films via self-assembly of block copolymers. *Adv. Mater.* **2002**, *14*, 1579−1583.

(11) Ahn, H.; Park, S.; Kim, S. W.; Yoo, P. J.; Ryu, D. Y.; Russell, T. P. Nanoporous block copolymer membranes for ultrafiltration: A simple approach to size tunability. *ACS Nano* **2014**, *8*, 11745−11752.

(12) Lazzari, M.; López-Quintela, M. A. Block Copolymers as a Tool for Nanomaterial Fabrication. *Adv. Mater.* **2003**, *15* (19), 1583−1594.

(13) Kim, J. K.; Yang, S. Y.; Lee, Y.; Kim, Y. Functional nanomaterials based on block copolymer self-assembly. *Prog. Polym. Sci.* **2010**, *35*, 1325−1349.

(14) Lodge, T. P.; Pudil, B.; Hanley, K. J. The full phase behavior for block copolymers in solvents of varying selectivity. *Macromolecules* **2002**, *35*, 4707−4717.

(15) Hanley, K. J.; Lodge, T. P.; Huang, C. I. Phase behavior of a block copolymer in solvents of varying selectivity. *Macromolecules* **2000**, *33*, 5918−5931.

(16) Battaglia, G.; Ryan, A. J. Effect of amphiphile size on the transformation from a lyotropic gel to a vesicular dispersion. *Macromolecules* **2006**, *39*, 798−805.

(17) Barnhill, S. A.; Bell, N. C.; Patterson, J. P.; Olds, D. P.; Gianneschi, N. C. Phase diagrams of polynorbornene amphiphilic block copolymers in solution. *Macromolecules* **2015**, *48*, 1152−1161.

(18) Gadelle, F.; Koros, W. J.; Schechter, R. S. Solubilization of aromatic solutes in block copolymers. *Macromolecules* **1995**, *28*, 4883−4892.

(19) Sakai, T.; Alexandridis, P. Single-step synthesis and stabilization of metal nanoparticles in aqueous pluronic block copolymer solutions at ambient temperature. *Langmuir* **2004**, *20*, 8426−8430.

(20) Peters, R. J.; Louzao, I.; Van Hest, J. C. From polymeric nanoreactors to artificial organelles. *Chem. Sci.* **2012**, *3*, 335−342.

(21) Kataoka, K.; Harada, A.; Nagasaki, Y. Block copolymer micelles for drug delivery: Design, characterization and biological significance. *Adv. Drug Delivery Rev.* **2012**, *64*, 37−48.

(22) Bose, A.; Burman, D. R.; Sikdar, B.; Patra, P. Nanomicelles: Types, properties and applications in drug delivery. *IET Nanobiotechnol.* **2021**, *15* (1), 19−27.

(23) Hamley, I. W. *Block copolymers in solution: fundamentals and applications*; John Wiley & Sons, 2005.

(24) Owen, S. C.; Chan, D. P.; Shoichet, M. S. Polymeric micelle stability. *Nano Today* **2012**, *7*, 53−65.

(25) Kelley, E. G.; Albert, J. N. L.; Sullivan, M. O.; Epps, T. H. Stimuli-responsive copolymer solution and surface assemblies for biomedical applications. *Chem. Soc. Rev.* **2013**, *42* (17), 7057−7071.

(26) Allen, T. M. Ligand-targeted therapeutics in anticancer therapy. *Nat. Rev. Cancer* **2002**, *2*, 750−763.

(27) Ruiz, A. L.; Ramirez, A.; McEnnis, K. Single and Multiple Stimuli-Responsive Polymer Particles for Controlled Drug Delivery. *Pharmaceutics* **2022**, *14* (2), 421.

(28) Hadjichristidis, N.; Pitsikalis, M.; Iatrou, H. Synthesis of Block Copolymers. *Adv. Polym. Sci.* **2005**, *189*, 1−124.

(29) Gitsov, I. Hybrid linear dendritic macromolecules: From synthesis to applications. *J. Polym. Sci., Part A: Polym. Chem.* **2008**, *46*, 5295−5314.

(30) Wurm, F.; Frey, H. Linear-dendritic block copolymers: The state of the art and exciting perspectives. *Prog. Polym. Sci.* **2011**, *36*, 1−52.

(31) Fan, X.; Zhao, Y.; Xu, W.; Li, L. Linear-dendritic block copolymer for drug and gene delivery. *Mater. Sci. Eng.* **2016**, *62*, 943−959.

(32) Whitton, G.; Gillies, E. R. Functional aqueous assemblies of linear-dendron hybrids. *J. Polym. Sci., Part A: Polym. Chem.* **2015**, *53*, 148−172.

(33) Liu, X.; Gitsov, I. Nonionic Amphiphilic Linear Dendritic Block Copolymers. Solvent-Induced Self-Assembly and Morphology Tuning. *Macromolecules* **2019**, *52*, 5563−5573.

(34) Lebedeva, I. O.; Zhulina, E. B.; Borisov, O. V. Theory of Linear-Dendritic Block Copolymer Micelles. *ACS Macro Lett.* **2018**, *7*, 42−46.

(35) Tomalia, D.; Baker, H.; Dewald, J.; Hall, M.; Kallos, G.; Martin, S.; Roeck, J.; Ryder, J.; Smith, P. A New class of polymers: Starburst-dendritic macromolecules. *Polym. J.* **1985**, *17*, 117−132.

(36) Grayson, S. M.; Fréchet, J. M. Divergent synthesis of dendronized poly(p-hydroxystyrene) [6]. *Macromolecules* **2001**, *34*, 6542−6544.

(37) Nuhn, L.; Schüll, C.; Frey, H.; Zentel, R. Combining ring-opening multibranching and RAFT polymerization: Multifunctional linear-hyperbranched block copolymers via hyperbranched macro-chain-transfer agents. *Macromolecules* **2013**, *46*, 2892−2904.

(38) Oikawa, Y.; Lee, S.; Kim, D. H.; Kang, D. H.; Kim, B.-S.; Saito, K.; Sasaki, S.; Oishi, Y.; Shibasaki, Y. One-pot synthesis of linear-hyperbranched amphiphilic block copolymers based on polyglycerol derivatives and their micelles. *Biomacromolecules* **2013**, *14*, 2171−2178.

(39) Cuneo, T.; Gao, H. Recent advances on synthesis and biomaterials applications of hyperbranched polymers. *WRES - Nanomed. Nanobiotechnol.* **2020**, *12* (6), No. e1640.
(40) Uhrich, K. E.; Hawker, C. J.; Fréchet, J. M. J.; Turner, S. R. One-Pot Synthesis of Hyperbranched Polyethers. *Macromolecules* **1992**, *25*, 4583−4587.
(41) Kim, Y. H.; Webster, O. W. Water soluble hyperbranched polyphenylene:" a unimolecular micelle?". *J. Am. Chem. Soc.* **1990**, *112*, 4592−4593.
(42) Andresen, T. L.; Larsen, J. B. Compositional inhomogeneity of drug delivery liposomes quantified at the single liposome level. *Acta Biomater.* **2020**, *118*, 207−214.
(43) Schmitt, A. L.; Repollet-Pedrosa, M. H.; Mahanthappa, M. K. Polydispersity-driven block copolymer amphiphile self-assembly into prolate-spheroid micelles. *ACS Macro Lett.* **2012**, *1*, 300−304.
(44) Barriau, E.; García Marcos, A.; Kautz, H.; Frey, H. Linear-Hyperbranched Amphiphilic AB Diblock Copolymers Based on Polystyrene and Hyperbranched Polyglycerol. *Macromol. Rapid Commun.* **2005**, *26*, 862−867.
(45) Mantha, S.; Qi, S.; Barz, M.; Schmid, F. How ill-defined constituents produce well-defined nanoparticles: Effect of polymer dispersity on the uniformity of copolymeric micelles. *Phys. Rev. Mater.* **2019**, *3*, 026002.
(46) Degennes, P. Macromolecules and Liquid Crystals: Reflections on Certain Lines of Research. *Liq. Cryst.* **1978**, 1−18.
(47) Noolandi, J.; Hong, K. M. Theory of Block Copolymer Micelles in Solution. *Macromolecules* **1983**, *16*, 1443−1448.
(48) Leibler, L.; Orland, H.; Wheeler, J. C. Theory of critical micelle concentration for solutions of block copolymers. *J. Chem. Phys.* **1983**, *79*, 3550−3557.
(49) Leermakers, F. A. M.; Wijmans, C. M.; Fleer, G. J. On the Structure of Polymeric Micelles: Self-Consistent-Field Theory and Universal Properties for Volume Fraction Profiles. *Macromolecules* **1995**, *28*, 3434−3443.
(50) Nelson, P. H.; Rutledge, G. C.; Hatton, T. A. On the size and shape of self-assembled micelles. *J. Chem. Phys.* **1997**, *107*, 10777−10781.
(51) Zhulina, E. B.; Borisov, O. V. Theory of Block Polymer Micelles: Recent Advances and Current Challenges. *Macromolecules* **2012**, *45*, 4429−4440.
(52) Wang, Y.; Li, B.; Zhou, Y.; Lu, Z.; Yan, D. Dissipative particle dynamics simulation study on the mechanisms of self-assembly of large multimolecular micelles from amphiphilic dendritic multiarm copolymers. *Soft Matter* **2013**, *9*, 3293−3304.
(53) Lebedeva, I. O.; Zhulina, E. B.; Borisov, O. V. Self-Assembly of Linear-Dendritic and Double Dendritic Block Copolymers: From Dendromicelles to Dendrimersomes. *Macromolecules* **2019**, *52*, 3655−3667.
(54) Brito, M. E.; Mikhtaniuk, S. E.; Neelov, I. M.; Borisov, O. V.; Holm, C. Implicit-Solvent Coarse-Grained Simulations of Linear-Dendritic Block Copolymer Micelles. *Int. J. Mol. Sci.* **2023**, *24*, 2763.
(55) Tan, H.; Wang, W.; Yu, C.; Zhou, Y.; Lu, Z.; Yan, D. Dissipative particle dynamics simulation study on self-assembly of amphiphilic hyperbranched multiarm copolymers with different degrees of branching. *Soft Matter* **2015**, *11*, 8460−8470.
(56) Tan, H.; Yu, C.; Lu, Z.; Zhou, Y.; Yan, D. A dissipative particle dynamics simulation study on phase diagrams for the self-assembly of amphiphilic hyperbranched multiarm copolymers in various solvents. *Soft Matter* **2017**, *13*, 6178−6188.
(57) Tan, H.; Li, S.; Li, K.; Yu, C.; Lu, Z.; Zhou, Y. Shape Transformations of Vesicles Self-Assembled from Amphiphilic Hyperbranched Multiarm Copolymers via Simulation. *Langmuir* **2019**, *35*, 6929−6938.
(58) Hao, T.; Tan, H.; Li, S.; Wang, Y.; Zhou, Z.; Yu, C.; Zhou, Y.; Yan, D. Multilayer onion-like vesicles self-assembled from amphiphilic hyperbranched multiarm copolymers via simulation. *J. Polym. Sci.* **2020**, *58*, 704−715.
(59) Gao, Z.; Eisenberg, A. A Model of Micellization for Block Copolymers in Solutions. *Macromolecules* **1993**, *26*, 7353−7360.
(60) Linse, P. Micellization of Poly(ethylene oxide)−Poly(propylene oxide) Block Copolymers in Aqueous Solution: Effect of Polymer Polydispersity. *Macromolecules* **1994**, *27*, 6404−6417.
(61) Lynd, N. A.; Meuler, A. J.; Hillmyer, M. A. Polydispersity and Block Copolymer Self-assembly. *Prog. Polym. Sci.* **2008**, *33* (9), 875−893.
(62) Doncom, K. E. B.; Blackman, L. D.; Wright, D. B.; Gibson, M. I.; O'Reilly, R. K. Dispersity effects in polymer self-assemblies: a matter of hierarchical control. *Chem. Soc. Rev.* **2017**, *46*, 4119−4134.
(63) Giannakou, M.; Borisov, O. V.; Schmid, F. Strong stretching theory of polydisperse curved polymer brushes. *J. Chem. Phys.* **2024**, *161* (1), 014903.
(64) Sunder, A.; Hanselmann, R.; Frey, H.; Mülhaupt, R. Controlled synthesis of hyperbranched polyglycerols by ring-opening multibranching polymerization. *Macromolecules* **1999**, *32*, 4240−4246.
(65) Schuell, C.; Rabbel, H.; Schmid, F.; Frey, H. Polydispersity and Molecular Weight Distribution of Hyperbranched Graft Copolymers via "Hypergrafting" of ABm Monomers from Polydisperse Macroinitiator Cores: Theory Meets Synthesis. *Macromolecules* **2013**, *46*, 5823−5830.
(66) Schmid, F. Self-consistent-field theories for complex fluids. *J. Phys.: Condens. Matter* **1998**, *10*, 8105−8138.
(67) Rabbel, H.; Frey, H.; Schmid, F. Statistical properties of linear-hyperbranched graft copolymers prepared via "hypergrafting" of ABm monomers from linear B-functional core chains: A molecular dynamics simulation. *J. Chem. Phys.* **2015**, *143* (24), 243125.
(68) Anderson, J. A.; Glaser, J.; Glotzer, S. C. HOOMD-blue: A Python package for high-performance molecular dynamics and hard particle Monte Carlo simulations. *Comput. Mater. Sci.* **2020**, *173*, 109363.
(69) Zimm, B. H. Apparatus and methods for measurement and interpretation of the angular variation of light scattering; preliminary results on polystyrene solutions. *J. Chem. Phys.* **1948**, *16*, 1099−1116.
(70) Sanchez, I. C.; Lacombe, R. H. Statistical Thermodynamics of Polymer Solutions. *Macromolecules* **1978**, *11*, 1145−1156.
(71) Grason, G. M.; Kamien, R. D. Self-consistent field theory of multiply branched block copolymer melts. *Phys. Rev. E* **2005**, *71*, 051801.
(72) Holm, C.; Kremer, K. *Advanced Computer Simulation Approaches for Soft Matter Sciences II*; Springer, 2005. DOI: .
(73) Yong, D.; Kim, J. U. Dynamic Programming for Chain Propagator Computation of Branched Block Copolymers in Polymer Field Theory Simulations. *J. Chem. Theory Comput.* **2025**, *21* (7), 3676−3690.
(74) Frey, H.; Hölter, D. Degree of branching in hyperbranched polymers. 3 Copolymerization of ABm-monomers with AB and ABn-monomers. *Acta Polym.* **1999**, *50*, 67−76.
(75) Hanselmann, R.; Hölter, D.; Frey, H. Hyperbranched Polymers Prepared via the Core-Dilution/Slow Addition Technique: Computer Simulation of Molecular Weight Distribution and Degree of Branching. *Macromolecules* **1998**, *31* (12), 3790−3801.
(76) Israelachvili, J. N.; Mitchell, D. J.; Ninham, B. W. Theory of self-assembly of hydrocarbon amphiphiles into micelles and bilayers. *J. Chem. Soc., Faraday Trans.* **1976**, *72*, 1525−1568.
(77) Hansen, C. M. *Hansen's Solubility Parameters: a User's Handbook*, 2 nd ed.; CRC Press, 2007.
(78) Zhang, X.; Jackson, J. K.; Burt, H. M. Development of amphiphilic diblock copolymers as micellar carriers of taxol. *Int. J. Pharm.* **1996**, *132*, 195−206.
(79) Zhu, X.; Zhou, Y.; Yan, D. Influence of Branching Architecture on Polymer Properties. *J. Polym. Sci. Part B − Polym. Phys.* **2011**, *49*, 1277−1286.
(80) Qiao, L.; Giannakou, M.; Schmid, F. An Efficient and Accurate SCF Algorithm for Block Copolymer Films and Brushes Using Adaptive Discretizations. *Polymers* **2024**, *16* (9), 1228.
(81) Wang, R.; Wang, Z.-G. Theory of Polymers in Poor Solvent: Phase Equilibrium and Nucleation Behavior. *Macromolecules* **2012**, *45*, 6266−6271.

https://doi.org/10.1021/acs.macromol.5c00615
Macromolecules 2025, 58, 5872−5882